Calcium–Dependent Conformation of a Heme and Fingerprint Peptide of the Diheme Cytochrome c Peroxidase from Paracoccus pantotrophus †

6 AUTHORS, INCLUDING:

Sofia R Pauleta
New University of Lisbon
51 PUBLICATIONS   363 CITATIONS

SEE PROFILE

Celia F Goodhew
The University of Edinburgh
27 PUBLICATIONS   635 CITATIONS

SEE PROFILE

Isabel Moura
New University of Lisbon
228 PUBLICATIONS   5,867 CITATIONS

SEE PROFILE

John A Shelnutt
University of Georgia
265 PUBLICATIONS   8,771 CITATIONS

SEE PROFILE

Calcium-Dependent Conformation of a Heme and Fingerprint Peptide of the Diheme Cytochrome c Peroxidase from *Paracoccus pantotrophus*[†]

Sofia R. Pauleta,[‡,§] Yi Lu,[‖,⊥] Celia F. Goodhew,[§] Isabel Moura,[‡] Graham W. Pettigrew,[§] and John A. Shelnutt*[,‖,⊥]

Centro de Química Fina e Biotecnologia, Departamento de Química, Faculdade de Ciências e Tecnologia, Universidade Nova de Lisboa, 2825 Monte de Caparica, Portugal, Department of Preclinical Veterinary Sciences, Royal (Dick) School of Veterinary Studies, The University of Edinburgh, Summerhall, Edinburgh EH9 1QH, U.K., Biomolecular Materials and Interfaces Department, Sandia National Laboratories, Albuquerque, New Mexico 87185-1349, and Department of Chemistry, The University of New Mexico, Albuquerque, New Mexico 87131

ABSTRACT: The structural changes in the heme macrocycle and substituents caused by binding of Ca^{2+} to the diheme cytochrome c peroxidase from *Paracoccus pantotrophus* were clarified by resonance Raman spectroscopy of the inactive fully oxidized form of the enzyme. The changes in the macrocycle vibrational modes are consistent with a Ca^{2+}-dependent increase in the out-of-plane distortion of the low-potential heme, the proposed peroxidatic heme. Most of the increase in out-of-plane distortion occurs when the high-affinity site I is occupied, but a small further increase in distortion occurs when site II is also occupied by Ca^{2+} or Mg^{2+}. This increase in the heme distortion explains the red shift in the Soret absorption band that occurs upon Ca^{2+} binding. Changes also occur in the low-frequency substituent modes of the heme, indicating that a structural change in the covalently attached fingerprint pentapeptide of the LP heme occurs upon Ca^{2+} binding to site I. These structural changes may lead to loss of the sixth ligand at the peroxidatic heme in the semireduced form of the enzyme and activation.

Cytochrome c peroxidase (CCP)[1] from *Paracoccus pantotrophus*, previously named as *Paracoccus denitrificans* (*1*), is a periplasmic diheme enzyme that catalyzes the reduction of hydrogen peroxide to water (*2*). This enzyme has similarities with the cytochrome c peroxidase from *Pseudomonas aeruginosa* (*3−7*), which is the other extensively characterized bacterial CCP. The three-dimensional structure of the latter was solved by X-ray crystallography (*8*) and consists of two domains, each containing a heme c. One heme, located in the C-terminal domain, is proposed to be an electron-transferring heme and the other, in the N-terminal region, is the peroxidatic heme. Similarly, *P. pantotrophus* CCP has two heme c domains (*9*) (Figure 1) with different redox potentials, which were estimated by redox titration of the UV−visible absorption spectrum to be −150 mV (low-potential heme) and +226 mV (high-potential heme) (*2*).

In the oxidized form, a methionine and a histidine side chain coordinate the HP heme, which is in a high/low-spin state equilibrium (*2*). The LP heme is low spin and coordinated by two histidines. This fully oxidized form of the enzyme is inactive but becomes active when semireduced with ascorbate (*2*) in the presence of calcium ion. In the semireduced form, the LP heme becomes high-spin five-coordinate and is accessible by hydrogen peroxide, while the high-potential heme is low spin and remains six-coordinate. This initial report focuses on the fully oxidized form of *P. pantotrophus* (*Pa-p*) CCP.

The presence of calcium ion has also been detected in other peroxidases such as horseradish peroxidase (*10*), lignin peroxidase (*11*), and *Ps. aeruginosa* (*Ps-a*) CCP (*8*), where it seems to be associated with the maintenance of the three-dimensional structure of these enzymes. For *Pa-p* CCP, the calcium ions are important for activation of the enzyme. Different spectroscopic techniques have shown that the enzyme has two Ca^{2+} binding sites with different affinities. Site I is proposed to be located between the two hemes of the monomer (in analogy with the site found in the three-dimensional structure of *Ps-a* CCP) and has a K_D of 1.2 μM in either the oxidized or the semireduced form (*12*). This site is always occupied at pH 6.0 or 7.5 because of residual calcium in the enzyme preparations. The enzyme has to be treated with a chelating agent, like EGTA, to remove this residual calcium. Calcium binding site II has been suggested to be located at the dimer interface. This calcium ion may be coordinated by residues 72−79 (Figure 1) (*9*). Site II has binding constants that are redox-dependent; in the oxidized form at pH 6.0, the affinity is very low with a K_D of 520 μM, but Ca^{2+} affinity increases in the semireduced form of the enzyme to a K_D of 3 μM. Due to its location, occupation

---

* To whom correspondence should be addressed. E-mail: jasheln@unm.edu. Phone: 505-272-7160. Fax: 505-272-7077.
‡ Universidade Nova de Lisboa.
§ The University of Edinburgh.
‖ Sandia National Laboratories.
⊥ The University of New Mexico.

[1] Abbreviations: CCP, cytochrome c peroxidase; EGTA, ethylene glycol bis(β-aminoethyl ether)-*N,N,N′,N′*-tetraacetic acid; HP, high potential; HS, high spin; LP, low potential; LS, low spin; *Pa-p*, *Paracoccus pantotrophus*; *Ps-a*, *Pseudomonas aeruginosa*; RR, resonance Raman.
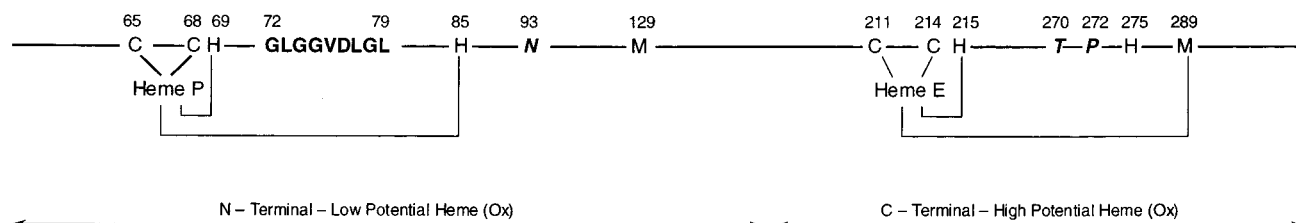
FIGURE 1: Schematic representation of the amino acid sequence of *P. pantotrophus* CCP [heme site attachments, heme ligands, conserved amino acids, and proposed calcium binding site I (bold and italic) and site II (bold)].

of site II is suggested to promote the dimerization of the CCP, which is essential for activation. This site differs from site I, in that it is empty at pH 7.5 and only partially occupied at pH 6.0 in fully oxidized protein preparations without added Ca^{2+}. Site II can also be occupied by magnesium or manganese ions (*12*).

There are two proposed mechanisms for the activation of the cytochrome c peroxidase based on all of the spectroscopic and electrochemical data collected, and until now, there is not enough experimental evidence to determine which model is more plausible. In the first of the models, the electron-transferring heme (C-terminal) and the peroxidatic heme (N-terminal) are the high-potential and low-potential hemes, respectively. In the semireduced form when the enzyme becomes active, these hemes are low spin and high spin, respectively, and the LP high-spin heme loses its histidine sixth ligand. In contrast in the second model, upon reduction of the HP heme, drastic modifications of the coordination spheres of the both hemes occur; the axial His85 ligand of the LP heme is replaced by Met129 (a conserved residue) and the methionine sixth ligand of the HP heme is lost. This change would stabilize the reduced form of the previously LP heme in that its redox potential increases enough to allow a spontaneous electron transfer from the HP heme at the C-terminus. So, in this model the semireduced form of the enzyme ends up with a low-spin six-coordinate configuration at the N-terminal heme and a high-spin five-coordinate configuration at the C-terminal heme. Thus, the latter heme functions as a peroxidatic heme and the former functions as an electron-transferring heme. Because the second model requires drastic modification at both hemes, the first model is currently favored.

Resonance Raman spectroscopy is a valuable probe of the vibrations of the heme and its local environment within proteins. In this work, we have used resonance Raman spectroscopy to determine the effect of calcium binding on the hemes and their binding sites in the oxidized form of *Paracoccus* cytochrome c peroxidase. Unlike UV−visible spectroscopy for example, resonance Raman spectroscopy provides detailed information about the specific structural changes in the heme that are associated with calcium binding. In particular, resonance Raman spectroscopy is sensitive to changes in spin state, axial coordination, oxidation state, out-of-plane distortion of the macrocycle, and conformational changes in the heme substituents, especially the thioether linkage of the heme-linked peptide that causes the characteristic distortion of c-type hemes (*13*). Since we have eliminated spin state, axial ligation, and oxidation state changes by our choice of solution conditions for the protein, resonance Raman spectroscopy can address the specific question of whether calcium binding influences the confor-

mation of the heme, the covalently linked fingerprint peptide, and other heme substituent groups. A Ca^{2+}-dependent conformational change in the heme macrocycle could provide a way for the protein to modulate the peroxidase activity and/or electron transport processes.

In past studies of other c-type cytochromes including mitochondrial cytochromes c and tetraheme cytochromes c_3, resonance Raman spectroscopy and computational studies have demonstrated that the characteristic out-of-plane distortion of the heme that is observed in X-ray crystal structures is a consequence of the interaction of the heme with the covalently attached fingerprint peptide (**CXXCH** or **CX-XXXCH**) (*14−17*). For the cytochromes c_3, the protein-induced ruffling appears to provide a mechanism, along with other factors, by which the protein modulates the redox potentials of the hemes (*17*). For c_3 proteins, a trend toward more negative Fe(III)/Fe(II) reduction potentials with increasing magnitude of ruffling has been reported (*17*), and further, model compound studies have shown a similar influence of ruffling on the redox potentials of the porphyrin macrocycle (*18−20*). Thus, calcium-dependent modulation of the heme conformation may also alter electron-transfer properties of *Pa-p* CCP such as the redox potentials of the hemes. For the mitochondrial cytochromes c, interaction of the heme with the fingerprint peptide results in a mainly ruffled deformation of the porphyrin macrocycle, but smaller waved deformations are also conserved. This is the typical heme distortion that is observed when only two amino acids intervene between the cysteines of the fingerprint peptide, as is the case for *Pa-p* CCP. In studies of microperoxidase-11 (*16*), we have also shown that the hydrophobicity of the environment of the heme-linked peptide is important for maintaining the nonplanar distortion of the macrocycle, and changes in the heme-linked peptide environment that occur when donor/acceptor proteins bind may influence the conformation of the fingerprint peptide and the resultant conformation of the heme. Thus, protein binding events also could potentially be coupled to heme structural changes, redox properties, electron transfer, and peroxidase activity.

Herein, we report the Ca^{2+}-dependent structural changes in the linkage to the fingerprint peptide and the heme macrocycle for the fully oxidized form of *Paracoccus* cytochrome c peroxidase. Calcium-dependent structural changes in the semireduced and fully reduced forms determined by resonance Raman spectroscopy are more complex and will be reported subsequently.

MATERIALS AND METHODS

Purification of Cytochrome c Peroxidase. Cytochrome c peroxidase was purified from *P. pantotrophus* (LMD 52.44) as previously described (*21*). Concentrated stocks of protein

in 5 mM MES, pH 6.0, and 10 mM NaCl were stored at −40 °C. Enzyme concentration was determined using an extinction coefficient at 408 nm for the monomer of 250 mM^{-1} cm^{-1}.

Preparation of Cytochrome c Peroxidase for RR Spectroscopy. In RR experiments, CCP was diluted from the stock solutions in 5 mM MES, pH 6.0, and 10 mM NaCl to 50, 10, or 5 μM and aged for 30 min to allow any monomer formation due to the dilution to occur. A Centricon apparatus was used to change the buffer of the protein to 5 mM HEPES, pH 7.5, and 10 mM NaCl. To obtain the protein with all the sites filled, either Ca^{2+} ($CaCl_2$) or Mg^{2+} ($MgCl_2$) was added to a concentration of 2 mM, and the protein was incubated for 60 min at 4 °C. The protein free of calcium was obtained by incubating the CCP solution with EGTA, 2 mM, for 60 min at 4 °C. Ionic strength was altered by adding NaCl to a final concentration of 16 mM for the untreated protein. For the EGTA-treated protein, the oxidized protein was incubated with NaCl for 60 min at a final concentration of 22 mM. In all of the experiments, the protein was fully oxidized by adding a solution of potassium ferricyanide.

Resonance Raman Spectroscopy. RR spectra were obtained using the 406.7 nm line of an INNOVA Kr^+ laser (Coherent). The spectrometer was a 0.75 m monochromator (Instruments, SA) with a 512 × 2048 pixel CCD detector. The slit width of 75 μm for the 2400 groove/mm holographic grating gives a spectral resolution of 2 cm^{-1}. The CCD array was cooled by LN2 to 138 K and controlled by a CCD3000 controller unit (Instruments, SA). The pixel columns of the CCD array chip (EEV) were binned to give 2048 13.5-μm channels or 0.4 cm^{-1} per channel near 400 nm. The chip is back-illuminated and has visible/NIR antireflection coatings. The spectrometer was interfaced to a 400 MHz Pentium II-based personal computer via an IEEE 488.2 PCI-GPIB interface card (National Instruments), and SpectraMax for Windows software (Instruments, SA) was used to collect the data from the CCD and to control the spectrometer. Position mode was used for CCD detection covering about 500 cm^{-1} of the Raman spectrum without moving the grating. Spectra were output as even-*X* ASCII files for plotting with SigmaPlot (SPSS). Polarized spectra were obtained using an oriented Polaroid sheet located between the notch filter and the scrambler.

Raman samples were kept in ice until the spectra were obtained, typically at room temperature (23 °C) in 2−10 min using 15 mW of partially focused laser power. Absorption spectra were obtained before and after the Raman spectra to ensure the integrity of the sample during laser irradiation.

RESULTS

The Raman spectra were obtained with 406.7 nm laser excitation, which is in resonance with the Soret band of the untreated oxidized protein. The Soret band is narrow and shows no evidence of the presence of two hemes with significantly different absorption spectra. Excitation at 413.1 nm does not give significantly altered RR spectra from those obtained at 406.7 nm and, specifically, does not appreciably alter the relative intensities of the high-spin and low-spin marker lines. Excitation at 406.7 nm enhances the mostly polarized totally symmetric A_{1g} and depolarized dynamic Jahn−Teller-active B_{1g} and B_{2g} in-plane vibrational modes,
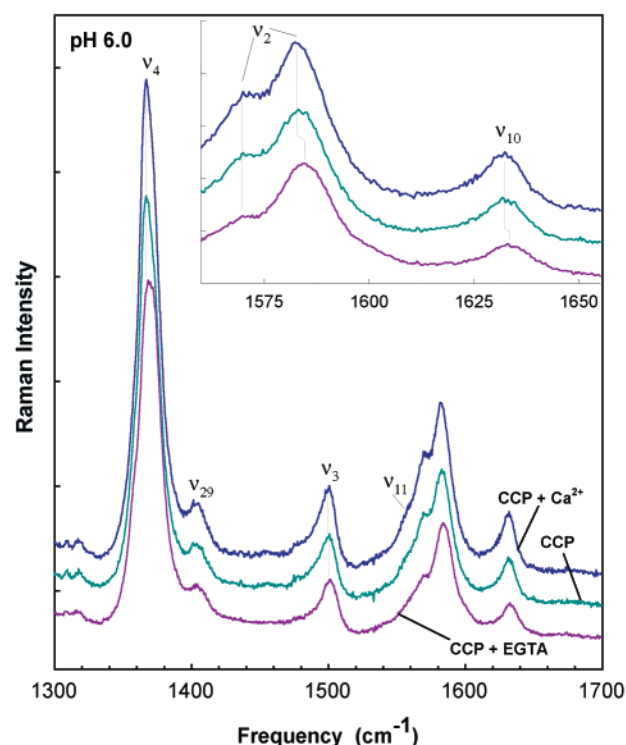

FIGURE 2: Resonance Raman spectrum of 50 μM *P. pantotrophus* CCP at pH 6.0 in the high-frequency region (a) with added calcium chloride, (b) as prepared, and (c) with added EGTA.

FIGURE 3: Resonance Raman spectrum of 10 μM *P. pantotrophus* CCP at pH 7.5 in the high-frequency region (a) with added magnesium chloride, (b) with added calcium chloride, (c) as prepared, and (d) with added EGTA.

which are particularly evident in the high-frequency region (Figures 2 and 3). The asymmetry introduced by macrocycle substituents and out-of-plane macrocycle distortion activates many in-plane and out-of-plane modes and substituent modes

FIGURE 4: Resonance Raman spectrum of *P. pantotrophus* CCP at 50 μM and pH 6.0 in the low-frequency region (a) with added calcium chloride, (b) as prepared, and (c) with added EGTA.
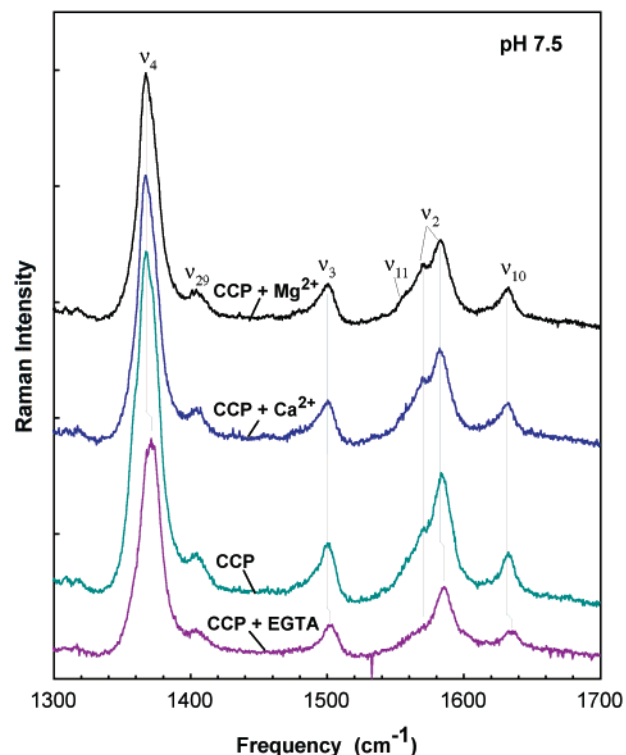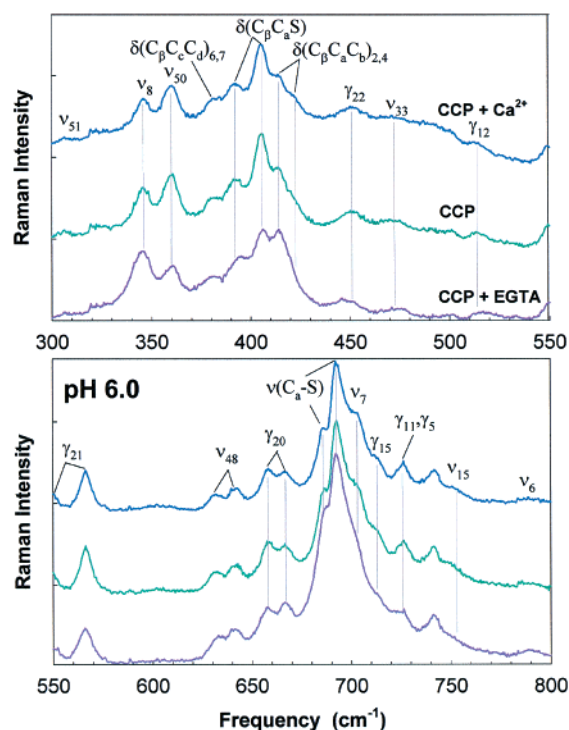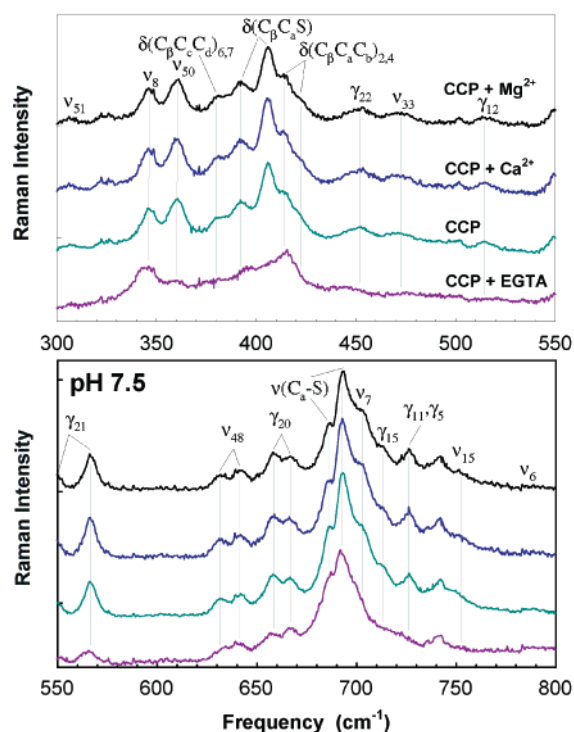

FIGURE 5: Resonance Raman spectrum of *P. pantotrophus* CCP at 10 μM and pH 7.5 in the low-frequency region (a) with added magnesium chloride, (b) with added calcium chloride, (c) as prepared, and (d) with added EGTA.

as well. These are most evident in the low-frequency region (Figures 4 and 5).

Although many of the resonance Raman vibrations of the heme show no significant calcium ion dependence, some lines are sensitive to the presence of Ca^{2+} and Mg^{2+}. We illustrate in Figures 2–5 only the parts of the low- and high-

Table 1: Frequencies (cm^{-1}) of the Resonance Raman Lines of Various Forms of *P. pantotrophus* Cytochrome c Peroxidase at pH 6.0 and 7.5

vibrational modes	pH 6.0			pH 7.5			
	CcP	CcP + Ca	CcP + EGTA	CcP	CcP + Ca	CcP + Mg	CcP + EGTA
ν_{51} (E$_u$)	306	306	306	307	307	307	307
ν_8 (A$_{1g}$)	346	346	346	346	346	346	345
ν_{50} (E$_u$)^a	360	360	360	360	360	360	360
δ(C$_\beta$C$_c$C$_d$)$_{6,7}$	381	381	381	381	381	381	381
δ(C$_\beta$C$_a$S)	393	393	393	392	392	392	396
	405	405	406	406	406	406	?
δ(C$_\beta$C$_a$C$_b$)$_{2,4}$	414	414	414	414	414	414	416
	422	422	422	422	422	422	422
γ_{22} (E$_g$)^a	451	451	448	452	452	452	443
ν_{33} (B$_{2g}$)	472	472	474	472	472	472	
γ_{12} (B$_{1u}$)	513	513	518	515	515	515	
γ_{21} (E$_g$)^b	549	549	551	549	549	549	551
	566	566	566	566	566	566	566
ν_{48} (E$_u$)^b	632	632	633	632	632	632	
	642	642	641	642	642	642	
γ_{20} (E$_g$)^b	658	658	657	659	659	659	657
	666	666	666	667	667	667	668
ν(C$_a$-S)	686	686	686	687	687	687	687
	693	693	692	693	693	693	692
ν_7 (A$_{1g}$)	703	703	703	703	703	703	
γ_{15} (B$_{2u}$)	712	712	712	713	713	713	
γ_{11}(B$_{1u}$), γ_5(A$_{2u}$)^d	726	726	726	727	727	727	
ν_{16} (B$_{1g}$)	742	742	741	742	742	742	742
ν_{15} (B$_{1g}$)	753	753		753	753	753	
ν_6 (A$_{1g}$)	790	790	789	788	788	788	788
ν_4 (A$_{1g}$)	1368	1368	1370	1368	1368	1368	1372
ν_{29} (B$_{2g}$)	1405	1405	1405	1405	1405	1405	1405
$\nu_{3\,(A1g)}$	1501	1501	1502	1501	1501	1501	1503
ν_{11} (B$_{1g}$)	1556	1556	1556	1556	1556	1556	1556
ν_2 (A$_{1g}$), HS^c	1570	1570	1570	1570	1570	1570	
ν_2 (A$_{1g}$), LS	1583	1583	1585	1584	1583	1584	1586
ν_{10} (B$_{1g}$)	1632	1632	1634	1633	1633	1633	1635

^{a} Doublet with peak frequency given. ^{b} Doublet with both components given. ^{c} Mode of minor high-spin component. ^{d} Assignment partially made on the basis of spectra of the reduced forms.

frequency regions that contain modes that are sensitive to Ca^{2+} and Mg^{2+}. We should also remark that the spectra of the untreated *Pa-p* CCP at the two different pH values do not show differences in the positions or the intensities of the Raman lines. This simplifies the analysis of the results, since the only changes observed are those due to the calcium or magnesium binding. Finally, addition of NaCl to raise the ionic strength has no effect on the spectrum of the untreated and EGTA-treated protein.

High-Frequency Skeletal Vibrational Modes of the Heme. Figures 2 and 3 show Raman spectra of the cytochrome c peroxidase in the oxidized form at pH 6.0 and 7.5, and Table 1 lists the values of the line frequencies and normal mode assignments. The spectra in Figures 2 and 3 differ in the protein concentration in addition to pH; for the pH 6.0 spectra, the protein concentration is 50 μM, and for the pH 7.5 spectra, the protein is 10 μM. This region of the Raman spectrum is populated with the well-known structure-sensitive lines, especially lines that are sensitive to the oxidation state, spin state (22–25), and nonplanar distortions of the macrocycle (26–33). The lines observed are those of A$_{1g}$, B$_{1g}$, and B$_{2g}$ in-plane symmetries (using the D_{4h} symmetry classifications); polarized spectra of *Pa-p* CCP reveal none of the A$_{2g}$ modes that are sometimes observed in the high-frequency region (e.g., for ferrocytochrome c) for Soret

excitation wavelengths. These marker lines, including ν_4, ν_3, ν_2, and ν_{10}, have recently been shown to be much more sensitive to the ruffling deformation than to saddling for heme proteins (*17*) and for model nickel porphyrins (*34*), but their sensitivities to other types of deformations are unknown.

The frequencies of the structure-sensitive marker lines ν_4, ν_3, ν_2, and ν_{10} of *Paracoccus* CCP are in good agreement with what is expected for an oxidized low-spin heme. Nevertheless, this protein is known to have two hemes in different spin states, and the spin states do not change with pH. Close inspection of the spectra reveals that the vibrational modes of the high-spin fraction of the HP His-Met coordinated heme are present as low-frequency shoulders on the marker lines. The low intensity of these shoulders may be partly because enhancement of the lines associated with the high-spin hemes is weaker and partly because only a fraction of the high-potential hemes are high spin. Differences in relative resonance enhancement for the individual lines may explain why the high-spin line of ν_{10} is not observed, while the high-spin ν_2 is fairly strong. There is no change in the spin-state equilibrium with pH or calcium ion concentration, and accordingly, no significant change in the intensity of the high-spin shoulders on the marker bands is noted in Figures 2 and 3. There are small differences in the EGTA-treated spectra obtained at pH 6.0 and 7.5; these differences are a result of incomplete removal of calcium from site I (vide infra).

Low-Frequency Skeletal and Substituent Vibrational Modes of the Heme. Figures 4 and 5 show RR spectra of CCP in the low-frequency region at pH 6.0 and 7.5 and protein concentrations of 50 and 10 μM, respectively. The assignments indicated in the figures and in Table 1 were based on the strong similarity of the frequencies and intensities with those of the corresponding Raman lines of yeast ferro- and ferricytochrome *c* isoenzyme-1, which were successfully assigned on the basis of extensive isotopic substitutions and normal-coordinate analysis (*35*) of the heme group of cytochrome *c*. Lines in the 300−800 cm^{-1} region show some calcium-dependent changes, and these lines are assigned to in-plane and out-of-plane macrocycle modes as well as modes associated with the substituents. The obvious differences between the EGTA-treated spectra at pH 6.0 and 7.5 are probably a result of incomplete removal of Ca^{2+} from site I at pH 6.0 where the affinity of the protein is highest and EGTA is a less effective chelator. These pH differences are best illustrated by the changes in the $\delta(C_\beta C_a S)$ mode at 407 cm^{-1}.

It is tempting to attribute the Raman lines observed in this region to the low-potential, low-spin heme as was done in the high-frequency region since there is no clear evidence of shoulders or lines from the different spin states or two different hemes. Lorentzian decomposition of the low-frequency spectrum (not shown) does not indicate the need for more than a single set of lines for one heme, indicating that neither two low-spin forms nor a high-spin/low-spin mixture due to the spin state equilibrium is required to fit the spectra. Nevertheless, both hemes of CCP could be represented in the low-frequency spectra. The reason only one heme is apparently seen in the Raman spectrum in this region could be a result of the high degree of congestion of lines in this region and the lack of significant frequency shifts

with spin state or even with oxidation state (*35*).

DISCUSSION

P. pantotrophus cytochrome *c* peroxidase needs 1.5 calcium ions per monomer bound to two sites on the protein to become active. One of these Ca^{2+} sites, site I, is thought to be almost equidistant between the HP and LP heme based on the crystal structure of the related bacterial CCP from *Ps. aeruginosa*, which contains one Ca^{2+} per monomer. The X-ray structure of *Ps-a* CCP (*8*) showing calcium site I is illustrated in Figure 6. The location of site II is currently unknown, but it is proposed to be nearer the LP heme and near the interface between the subunits of the dimer (Figure 6a). Neither Ca^{2+} binding site is close enough to the hemes to directly influence their structure, but the heme conformation might be altered indirectly by calcium-induced changes in the protein structure.

To determine whether the binding of calcium ions does influence the conformation of the heme, the enzyme was incubated under different solution conditions. First, the choices for the pH are based on previous results that have shown that the occupancy of these two binding sites, in the oxidized form, is different at these two pH values. Site I is always occupied unless EGTA is added to extract the calcium bound to the high-affinity site I, but site II is only partially occupied at pH 6.0 and should be empty at pH 7.5 where the affinity for calcium is lower than at pH 6.0. This pH difference is inferred for the oxidized protein on the basis of spectroscopic measurements on the semireduced form and NMR measurements on the oxidized form (*12*). The conditions that were assayed at pH 6.0 (50 μM protein) and pH 7.5 (10 μM protein) were (a) no calcium occupying any of the sites (+EGTA), (b) site I occupied and site II partially occupied or site I occupied and site II empty (untreated at pH 6.0 or 7.5, respectively), and (c) sites I and II fully occupied (+Ca^{2+}).

The information about the heme structure contained in the RR spectra is primarily for the LP heme, which is low spin and consequently has a stronger RR spectrum than the mostly high-spin HP heme. Both hemes would be expected to be low spin on the basis of their His-His and His-Met coordination, but it is known from NMR and UV−visible spectroscopy that it is the HP His-Met heme that is mostly high spin (*2*). In addition, on comparison of the RR spectra of CCP (pH 7.5) + EGTA in the oxidized and semireduced forms, so that just the HP heme is reduced and goes from HS to LS, we find that the LP heme is always low spin (*36*).

Distortion of the Heme Macrocycle. The high-frequency RR results suggest that the LP heme becomes more nonplanar with the filling of site I with calcium ion and still more nonplanar as site II is filled. The increase in macrocycle nonplanarity upon filling site I is indicated by the decreases in the frequencies of the structure-sensitive lines ν_{10}, ν_2, ν_3, and ν_4 for the protein with added calcium relative to the EGTA-treated protein; the decreases are 2.5, 3.0, 1.5, and 3.8 cm^{-1}, respectively. A further small but reproducible decrease in the frequencies is seen when calcium is added to the untreated protein, indicating that filling site II further increases the out-of-plane deformation.

The deformation type that is changing upon calcium binding may be ruffling since the frequencies of the structure-
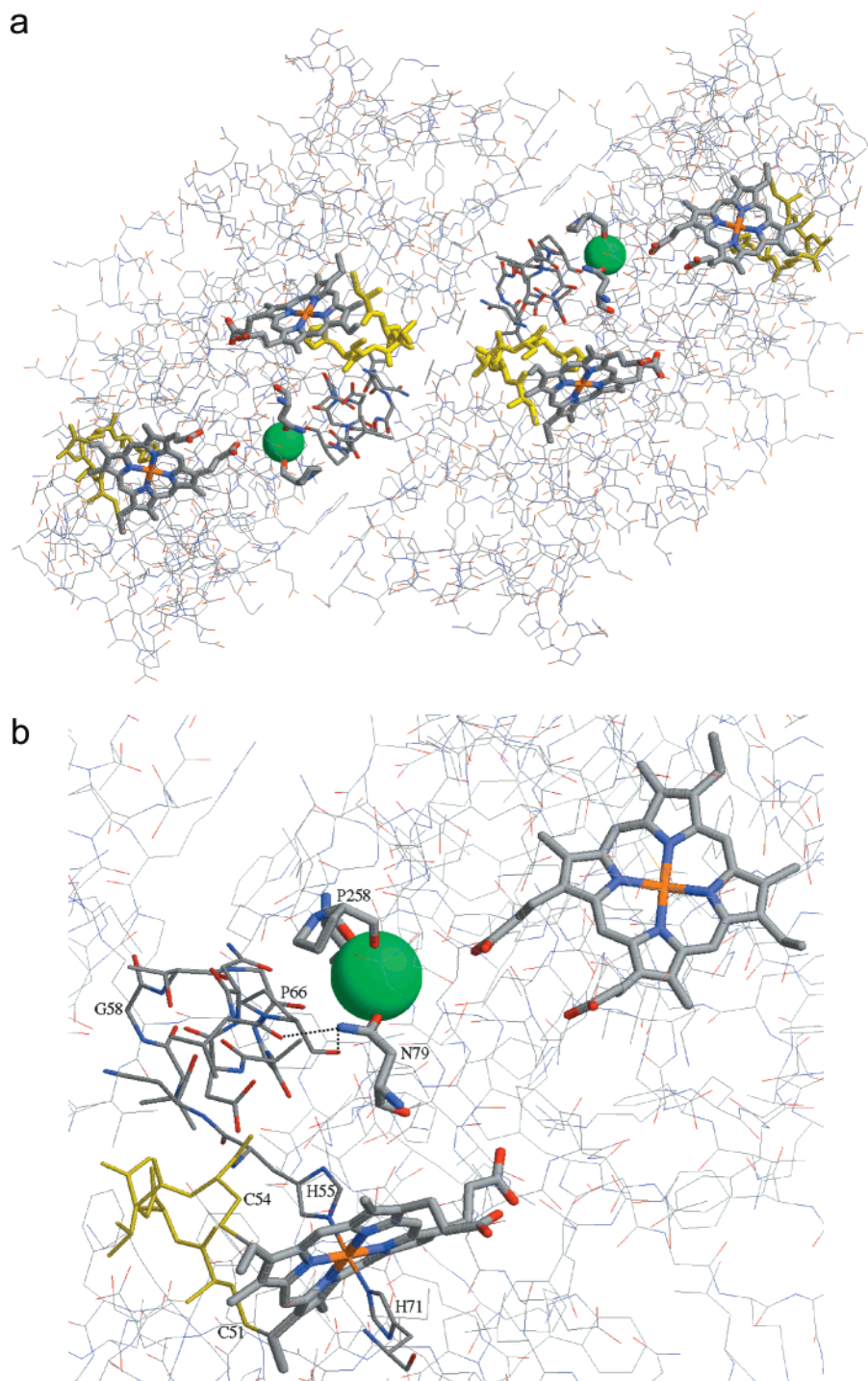
a

b

FIGURE 6: (a) X-ray structure of *Ps. aeruginosa* cytochrome c peroxidase. The fingerprint peptide is shown in yellow except for the proximal His55 (69 for *Pa-p*). The sequence from 55 to 66 is shown in CPK-colored thin sticks; the three residues coordinating to the Ca^{2+} ion (green) are shown as thick sticks in CPK colors. (b) The region of the proposed calcium binding sites is expanded, showing two hydrogen bonds to Asp79 (Asp93 for *Pa-p*), which is coordinated to the calcium (site I).

sensitive lines depend strongly upon the magnitude of this deformation type. On the other hand, a large increase in another type of deformation, e.g., saddling, could also account for the decreases in frequency. However, the increase in saddling, for example, would have to be large because saddling is known to cause much smaller decreases in marker line frequencies than an equivalent ruffling distortion (*37*). Other types of nonplanar deformation cannot be ruled out either. On the other hand, the low marker line frequencies for the low-spin heme (e.g., 1635 cm^{-1} for ν_{10} of the EGTA-treated protein) indicate a substantially nonplanar heme under

all solution conditions, and it is likely that a small increase in this already present heme deformation occurs, instead of or in addition to changes in the other types of deformation. If the deformation that causes the low marker line frequencies is predominantly ruffling, as is the case for most other c-type cytochromes, then the frequencies of the marker lines indicate a substantial ruffling of the LP heme. On the basis of the low frequencies for the LP heme of *Pa-p* CCP in the presence of calcium (1633 cm^{-1} for ν_{10}), the ruffling is even greater than that for the heme of yeast cytochrome c (Figure 7), which has ν_{10} at 1635 cm^{-1} (*35*). For comparison, ν_{10} of the
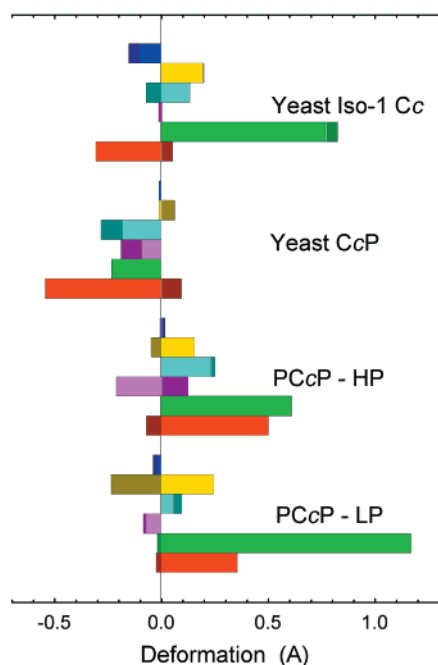
FIGURE 7: Normal-coordinate structural decompositions of the hemes of *Ps. aeruginosa* cytochrome *c* peroxidase (resolution: 2.4 Å), yeast cytochrome *c* peroxidase (PDB code 1cca; 1.8 Å), and yeast ferrocytochrome *c* (1ycc; 1.23 Å). Light colored bars give the deformations along the lowest frequency normal coordinate of each out-of-plane symmetry type [saddling (B_{2u}), red; ruffling (B_{1u}), green; doming (A_{2u}), pink; *x*-waving (E_{gx}), cyan; *y*-waving (E_{gy}), yellow; propellering (A_{1u}), blue]. Dark colors give the deformations along the next to lowest frequency mode of each symmetry type. The pure deformations are illustrated at http://jasheln.unm.edu/, and NSD results for over 1500 hemes in the Protein Data Bank are also available.

bis-His hemes *c* of cytochromes *c* of cytochromes c_3 range from 1640 cm^{-1} (near planar) to 1625 cm^{-1} (1.2 Å ruffling) (*17*). The suggestion that ruffling is the major deformation and also is larger for *Pa-p* CCP than for cytochrome *c* is in agreement with the crystal structure of the related CCP of *Pseudomonas aeruginosa*, which shows a ruffling of 1.2 Å for the low-spin heme compared with 0.8 Å for the ruffling for yeast ferrocytochrome *c*. (The saddling of the hemes of *Ps-a* CCP is significantly less than the ruffling: 0.4 and 0.5 Å, respectively, for *Pa-p* CCP and yeast cytochrome *c*.)

The RR spectra in the high-frequency region at low protein concentration and pH 7.5 (Figure 3) show changes upon calcium binding that are similar to the pH 6.0 spectra (Figure 2). It is expected that, at pH 7.5, site I is occupied and site II is empty for the protein without added EGTA or calcium. Close examination of the spectra in Figure 3 shows that lower marker line frequencies are observed when calcium ion is present (CCP and CCP + Ca^{2+}) than when not (+EGTA). Moreover, most of the frequency decrease comes from filling calcium site I, with only a small further decrease upon filling site II by adding calcium to the untreated protein. Addition of magnesium ion instead of calcium to fill site II appears to have the same influence on the macrocycle structure as adding calcium (Figure 3). In this case, calcium fills site I and magnesium fills site II.

Summarizing the RR results for the high-frequency region, the spectra at both pH values and concentrations are consistent with a significant increase in the nonplanar distortion of the heme macrocycle—probably in the amount of ruffling of the heme—upon the filling of Ca^{2+} site I. A further increase in the distortion occurs upon filling site II. Examination of the low-frequency RR spectra indicates how calcium binding is structurally linked to these identified changes in the heme macrocycle conformation (vide infra). These structural changes in the macrocycle also account for a change in the absorption spectrum that is observed upon calcium binding (*2*), specifically a red shift in the Soret band. A red shift is commonly observed upon increased ruffling of the porphyrin macrocycle (*31*).

The Raman spectral changes in the low-frequency region also support increased ruffling of the heme as calcium is added. In particular, the frequency of the in-plane totally symmetric metal—nitrogen(pyrrole) vibration (*35*) ν_8 is known to be influenced by ruffling (*16, 28*). For *Paracoccus* CCP, the frequency of the A_{1g} mode ν_8 at 346 cm^{-1} increases when site I is occupied by calcium (Figures 4 and 5), as is expected if the heme becomes more ruffled. This upshift for the untreated protein relative to the EGTA-treated protein may be more apparent in the pH 7.5 spectra (Figure 5) than in the pH 6.0 spectra (Figure 4), but the upshift is significant for both. No further apparent increase occurs with added Ca^{2+} or Mg^{2+}. In addition, there is certainly a dramatic increase in intensity of the neighboring ν_{50} vibrational mode at 360 cm^{-1}, an E_u in-plane mode that is activated by the distortion and asymmetric substitution of the heme. Both of these modes are assigned to the Fe—N(pyrrole) stretching and pyrrole substituent bending coordinates but differ in their phases.

The low-frequency region shown in Figures 4 and 5 is densely populated with lines assigned to substituent and out-of-plane vibrations (*35*) and thus potentially contains information about the specific nonplanar macrocycle deformation and the possible role that the substituents play in causing that distortion. The out-of-plane modes, in particular, are Raman active precisely because of the nonplanar heme distortion. A characteristic distortion is evident in nearly all of the X-ray crystal structures of *c*-type cytochromes. In fact, the most prevalent out-of-plane modes are of B_{1u} and E_g symmetry (in D_{4h}), and further deformations of these symmetries are precisely those that are the conserved nonplanar deformations of the hemes in mitochondrial cytochromes *c* (*16, 38, 39*). Specifically for yeast ferrocytochrome *c*, the observed B_{1u} modes are γ_{10}, γ_{11}, and γ_{12} appearing at 841, 724, and 540, respectively, and the prominent E_g modes are γ_{19}, γ_{20}, γ_{21}, and γ_{22} (*35*). The frequencies of the latter doubly degenerate modes are often split (e.g., γ_{20} at 653 and 666 cm^{-1} and γ_{21} at 552 and 568 cm^{-1}). A few lines of other out-of-plane symmetries are also observed; for example, γ_5 is an A_{2u} mode appearing at 729 cm^{-1}.

Figure 7 illustrates the macrocyclic deformations contributing to the out-of-plane distortions of the hemes in the crystal structure of *Ps. aeruginosa* CCP and compares them with the deformations contributing to the distortion of the hemes of yeast ferrocytochrome *c* isozyme-1 and yeast cytochrome *c* peroxidase. The symmetric deformations illustrated in Figure 7 are obtained by using normal-coordinate structural decomposition (NSD) (*38, 40*), a method for describing the distortion of the heme in terms of equivalent displacements along the normal coordinates of the macrocycle (see http://jasheln.unm.edu). In Figure 7, we

illustrate the deformations along the lowest (light color) as well as the next to lowest (dark color) frequency modes of each out-of-plane symmetry type. The major deformations are ruffling (green; B_{1u}), x- and y-waving (cyan and yellow; E_g), and saddling (red; B_{2u}). For a large group of c-type cytochrome crystal structures, only the positive ruffle and wave deformations are conserved. Not surprisingly, vibrations of the same symmetries as these conserved deformations (B_{1u} and E_g) appear prominently in the low-frequency Soret-excited Raman spectra of ferro- and ferricytochrome c (*35*).

For *Paracoccus* CCP, we see enhancements of the same out-of-plane vibrations of the heme in the low-frequency region as for yeast ferri- and ferrocytochrome c. Specifically, the B_{1u} modes that may be assigned are γ_{12} at 515 cm⁻¹, γ_{11} at 713 cm⁻¹, and a weak γ_{10} at 842 cm⁻¹ (not shown); the E_g modes that can be assigned are the doublets assigned to γ_{22} near 450 cm⁻¹, γ_{21} at 550 and 567 cm⁻¹, and γ_{20} at 659 and 668 cm⁻¹. The same lines are enhanced for CCP most likely because the structure of the LP heme has the characteristic heme conformation of other c-type hemes, which is composed of conserved B_{1u} (*ruf*) and E_g [*wav(x)* + *wav(y)*] deformations. Finally and most importantly, all of these lines show changes when Ca^{2+} or Mg^{2+} is present. For the E_g modes, the relative intensities of the lines making up the doublets change, and slight shifts are seen is some cases. For the B_{1u} modes γ_{12} and γ_{11}, the lines become weaker or virtually disappear when no Ca^{2+} is present.

In previous work (*17*), we have shown using molecular modeling and RR spectroscopy that the conserved distortions of the hemes in cytochrome c and tetraheme cytochromes c_3 are caused by the interaction of the heme with the covalently attached fingerprint peptide. The present CCP work provides direct evidence that changes in the conformation of the fingerprint peptide are associated with changes in the conformation of the heme. This can be seen by examining the substituent modes in the low-frequency region of the RR spectrum, which we now do.

Conformation of the Fingerprint Peptide and Heme Substituents. For cytochrome c, vibrational modes internal to the thioether linkages at the 2 and 4 positions of the heme are prominent in the RR spectra (*35*). These include the bending modes of the thioether linkages at 394 and 401 cm⁻¹ [$\delta(C_\beta C_a S)$] and at 413 and 421 cm⁻¹ [$\delta(C_\beta C_a C_b)$] for the reduced protein (12 K) and at 397 cm⁻¹ [$\delta(C_\beta C_a S)$] and at 412 and 418 cm⁻¹ [$\delta(C_\beta C_a C_b)$] for the oxidized protein (298 K). In addition, there are C_a-S stretching modes at 682 and 692 cm⁻¹ for ferrocytochrome c and at 693 cm⁻¹ for ferricytochrome c.

The corresponding thioether bending modes of oxidized *Pa-p* CCP are at 392 and 406 cm⁻¹ [$\delta(C_\beta C_a S)$] and at 414 and 422 cm⁻¹ [$\delta(C_\beta C_a C_b)_{2,4}$]; the corresponding C_a-S stretching modes are at 687 and 693 cm⁻¹ (Figures 4 and 5). All of these modes change significantly as site I is filled with Ca^{2+}. Especially sensitive are the modes of the bending motions involving the sulfur atoms near 400 cm⁻¹. These are some of the largest calcium-dependent changes in the RR spectrum. These spectral changes clearly indicate that changes in the conformation of the covalent linkage to the fingerprint peptide are associated with site I occupation.

A pair of bands at 372 and 382 cm⁻¹ for ferrocytochrome c and at 380 cm⁻¹ for ferricytochrome c and myoglobin is assigned to the propionate bending modes [$\delta(C_\beta C_c C_d)_{6,7}$] by propionate deuteration (*35, 41*). For *Paracoccus* CCP, these modes may be split in the absence of calcium as for cytochrome c but become a single mode at 381 cm⁻¹ when site I is occupied (Figures 4 and 5). No obvious additional changes occur upon filling site II.

Calcium Binding and Heme Conformational Changes. Figure 6 shows the X-ray crystal structure of the related CCP from *Ps. aeruginosa* (*8*). The calcium binding site, analogous to site I of *Paracoccus* CCP, is located approximately equidistant from the two hemes and near the interface between the subunits of the dimer. The calcium is not in a location suitable for interacting directly with either heme group. The most likely pathway for the binding of calcium at site I to be communicated to the LP heme is through a protein segment that has been proposed to comprise part of the second calcium site (*9*). This segment contains the proposed site II sequence that has been assigned on the basis of its similarity with the sequence of a Ca^{2+} binding site in β-roll proteins such as alkaline protease (*9, 42*). This site II segment consists of residues 58−65 (72−79 for *Pa-p*) within the segment indicated in Figure 6. This sequence of *Ps-a* is adjacent to the LP heme fingerprint peptide at residues 51−55 (65−69 for *Pa-p*). The segment from 56 to 66 has a β-sheet-like structure with extensive hydrogen bonding between the loops imparting considerable rigidity to this segment. Further, this segment is also H-bonded to residues that interact directly with the bound Ca^{2+} ion, residue Asp79 in particular. (Two H-bonds are indicated in Figure 6b.) Finally, the continuing sequence from 66 to 71 proceeds directly across the edge of the LP heme where His71 (His85 for *Pa-p*) forms the distal ligand to the iron atom of the LP heme. This arrangement provides a strongly coupled pathway for transmitting structural changes associated with calcium binding at site I to the fingerprint peptide and the LP heme group and its axial ligands.

From the spectral changes in the high-frequency region of the resonance Raman spectra of *Paracoccus* CCP, it is apparent that the macrocycle becomes more distorted when calcium binds to sites I and II, with the largest increase in distortion occurring with occupation of site I. The increase in distortion is in the LP bis-His heme since this is the heme that is observed in the high-frequency RR spectrum. Assuming that the calcium binding sites are at the proposed locations in the protein, it is not unexpected that the conformation of the LP heme would be influenced by calcium binding to either site. That is, one would expect that the change in distortion upon filling site I could be mediated by a change in the conformation of the fingerprint peptide since it is contained in the strong link between the calcium binding site and the LP heme. Because of the weakness of the high-frequency RR spectrum of the high-spin HP heme, it is not possible to tell whether the conformation of this heme is altered as well.

The calcium-dependent changes in the heme RR lines are consistent with the suggestion that the changes in the macrocycle out-of-plane distortion result from a conformational change in the fingerprint peptide of the LP heme. First, the vibrational modes belonging to the substituents at the 2 and 4 positions, especially those associated with bending of the cysteine sulfur atoms of the fingerprint peptide, show the largest calcium-dependent shifts and changes in intensity.

Second, the doming, ruffling, and waving out-of-plane modes of the heme, which are enhanced precisely because of the nonplanar deformations of these symmetry types caused by the fingerprint peptide, are also sensitive to calcium binding. Since the tension in the fingerprint peptide causes these particular deformations, a change in the conformation of this peptide segment would be expected to alter the vibrational modes associated with these macrocycle deformations. An alternative interpretation is that forces on the heme from sources not involving the fingerprint peptide increase the already present distortion, resulting in a Ca^{2+}-dependent increase and further changes to the fingerprint peptide linkage. A caveat to these interpretations is that for the low-frequency RR spectrum it is not clear that we are observing only the LP heme.

The detected changes in the propionate modes could be a consequence of the change in nonplanar distortion of the LP heme. On the other hand, the conformation of one propionate of the HP heme adjacent to site I might be altered by calcium binding (Figure 6b). Again, these two alternatives cannot be resolved at present because the RR lines in the low-frequency region could be a mixture of lines from both hemes.

The smaller increase in the macrocycle distortion that occurs upon calcium binding to site II does not show up as significant spectral changes in the low-frequency region. This could indicate that this macrocycle distortion results from interactions of the protein with the heme that are not transmitted through the fingerprint peptide. That is, occupation of site II causes changes in parts of the protein other than the fingerprint peptide that result in small changes in the macrocycle conformation that do not significantly alter the configuration of the covalently linked peptide.

CONCLUSIONS

The resonance Raman results add specific information about the protein and heme structural changes that occur upon calcium binding to *Paracoccus* CCP that is not obtainable from the UV−visible absorption spectra. Changes in the spectra upon filling calcium binding site I are consistent with an increase in the out-of-plane distortion of the low-potential heme. The most likely mechanism for causing this change in macrocycle distortion is a structural change in the pentapeptide **CQTCH** covalently linked to the LP heme. This calcium-dependent conformational change in the pentapeptide is evident from changes in the vibrational modes of the cysteine linkages and the out-of-plane modes of the macrocycle. It is unlikely that these structural changes occur at the HP heme because its fingerprint peptide is far from the proposed calcium binding sites. It remains possible, however, that other forces cause the Ca^{2+}-dependent increase in distortion and that the pentapeptide is just responding to the change in heme conformation.

The LP heme, the proposed peroxidatic heme, switches to the active five-coordinate high-spin state in the semireduced form of the enzyme only when Ca^{2+} is bound to both sites. Site I occupation causes a structural change in the LP heme and the fingerprint peptide, but in the fully oxidized enzyme, only a small increase in the heme out-of-plane distortion is detected when sites I and II are filled. Nevertheless, the Ca^{2+}-induced structural changes, detected in the fully

oxidized form, may result in strain at either the proximal or distal histidine ligands, which may increase in the semireduced form and result in ligand loss at one of the coordination positions. Moreover, in the semireduced active form, the affinity of calcium site II greatly increases, possibly enhancing the Ca^{2+}-dependent structural changes. These enhanced structural changes in the fingerprint peptide and the heme might then result in the loss of one of the distal ligands of the LP heme, possibly His71. The changes in conformation of the LP heme and its fingerprint pentapeptide may also contribute to redox potential changes.

All of the X-ray crystal structures of peroxidases show hemes that are predominately saddled (*34*). The only exceptions are the structures (3.5 to 4.0 Å resolution) of the bifunctional prostaglandin H synthase with bound inhibitors (*43*, *44*) and the structure of *Ps-a* CCP (2.4 Å resolution) (*8*). The distortions for prostaglandin H synthase structures may be in error because of the poor resolution or because of structural changes associated with occupation of the cyclooxygenase site. It will be of great interest to determine whether the LP heme becomes saddled in the five-coordinate semireduced form of the enzyme.

Resonance Raman spectroscopy of the semireduced and fully reduced forms of the enzyme provides additional information about the conformational changes that are associated with calcium binding and activation of the enzyme. Specifically, these studies, which are underway in our laboratories, shed additional light on the question of which heme becomes the five-coordinate one and the site of peroxidation.

REFERENCES

1. Rainey, F. A., Kelly, D. P., Stackebrandt, E., Burghardt, J., Hiraishi, A., Katayama, Y., and Wood, A. P. (1999) *Int. J. Syst. Bacteriol. 49*, 645−651.
2. Gilmour, R., Goodhew, C. F., Pettigrew, G. W., Prazeres, S., Moura, I., and Moura, J. J. G. (1993) *Biochem. J. 294*, 745−752.
3. Rönnberg, M., and Ellfolk, N. (1979) *Biochim. Biophys. Acta 581*, 325−333.
4. Rönnberg, M., Osterlund, K., and Ellfolk, N. (1980) *Biochim. Biophys. Acta 626*, 23−30.
5. Ellfolk, N., Rönnberg, M., Aasa, R., Andréasson, L. E., and Vänngård, T. (1983) *Biochim. Biophys. Acta 743*, 23−30.
6. Foote, N., Peterson, J., Gadsby, P. M., Greenwood, C., and Thomson, A. J. (1984) *Biochem. J. 223*, 369−78.
7. Samyn, B., Van Craenenbroeck, K., De Smet, L., Vandenberghe, I., Pettigrew, G., and Van Beeumen, J. (1995) *FEBS Lett. 377*, 145−149.
8. Fulop, V., Ridout, C. J., Greenwood, C., and Hajdu, J. (1995) *Structure (London) 3*, 1225−1233.
9. Hu, W., Van Driessche, G., Devreese, B., Goodhew, C. F., McGinnity, D. F., Saunders, N., Fulop, V., Pettigrew, G. W., and Van Beeumen, J. J. (1997) *Biochemistry 36*, 7958−7966.
10. Haschle, R. H., and Friedhoff, M. (1978) *Biochem. Biophys. Res. Commun. 80*, 1039−1042.
11. Poulos, T. L., Edwards, S. L., Wariishi, H., and Gold, M. H. (1993) *J. Biol. Chem. 268*, 4429−4440.
12. Gilmour, R., Prazeres, S., McGinnity, D. F., Goodhew, C. F., Moura, J. J. G., Moura, I., and Pettigrew, G. W. (1995) *Eur. J. Biochem. 234*, 878−886.
13. Ma, J. G., Zhang, J., Franco, R., Jia, S. L., Moura, I., Moura, J. J., Kroneck, P. M., and Shelnutt, J. A. (1998) *Biochemistry 37*, 12431−12442.
14. Hobbs, J. D., and Shelnutt, J. A. (1995) *J. Protein Chem. 14*, 19−25.

15. Ma, J. G., Laberge, M., Song, X. Z., Jentzen, W., Jia, S. L., Zhang, J., Vanderkooi, J. M., and Shelnutt, J. A. (1998) *Biochemistry 37*, 5118−5128.

16. Ma, J.-G., Vanderkooi, J. M., Zhang, J., Jia, S.-L., and Shelnutt, J. A. (1999) *Biochemistry 38*, 2787−2795.

17. Ma, J.-G., Zhang, J., Franco, R., Jia, S.-L., Moura, I., Moura, J. J. G., Kroneck, P. M. H., and Shelnutt, J. A. (1998) *Biochemistry 37*, 12431−12442.

18. Barkigia, K. M., Berber, M. D., Fajer, J., Medforth, C. J., Renner, M. W., and Smith, K. M. (1990) *J. Am. Chem. Soc. 112*, 8851−8857.

19. Barkigia, K. M., Chantranupong, L., Smith, K. M., and Fajer, J. (1988) *J. Am. Chem. Soc. 110*, 7566−7567.

20. D'Souza, F., Villard, A., Caemelbecke, E. V., Franzen, M., Boschi, R., Tagiagtesta, P., and Kadish, K. M. (1993) *Inorg. Chem. 32*, 4042.

21. Goodhew, C. F., Wilson, I. B. H., Hunter, D. J. B., and Pettigrew, G. W. (1990) *Biochem. J. 271*, 707−712.

22. Yamamoto, T., Palmer, G., Gill, D., Salmeen, I. T., and Rimai, L. (1973) *J. Biol. Chem. 248*, 5211.

23. Spiro, T. G., and Strekas, T. C. (1974) *J. Am. Chem. Soc. 96*, 338.

24. Spiro, T. G., and Burke, J. M. (1976) *J. Am. Chem. Soc. 98*, 5482−5489.

25. Spiro, T. G. (1982) in *Iron Porphyrins* (Lever, A. B. P., and Gray, H. B., Eds.) p 89, Addison-Wesley, Reading, MA.

26. Shelnutt, J. A., Medforth, C. J., Berber, M. D., Barkigia, K. M., and Smith, K. M. (1991) *J. Am. Chem. Soc. 113*, 4077−4087.

27. Shelnutt, J. A., Majumder, S. A., Sparks, L. D., Hobbs, J. D., Medforth, C. J., Senge, M. O., Smith, K. M., Miura, M., Luo, L., and Quirke, J. M. E. (1992) *J. Raman Spectrosc. 23*, 523−529.

28. Song, X. Z., Jentzen, W., Jia, S. L., Jaquinod, L., Nurco, D. J., Medforth, C. J., Smith, K. M., and Shelnutt, J. A. (1996) *J. Am. Chem. Soc. 118*, 12975−12988.

29. Song, X. Z., Jaquinod, L., Jentzen, W., Nurco, D. J., Jia, S. L., Khoury, R. G., Ma, J. G., Medforth, C. J., Smith, K. M., and Shelnutt, J. A. (1998) *Inorg. Chem. 37*, 2009−2019.

30. Song, X. Z., Jentzen, W., Jaquinod, L., Khoury, R. G., Medforth, C. J., Jia, S. L., Ma, J. G., Smith, K. M., and

31. Shelnutt, J. A. (1998) *Inorg. Chem. 37*, 2117−2128.

31. Jentzen, W., Simpson, M. C., Hobbs, J. D., Song, X., Ema, T., Nelson, N. Y., Medforth, C. J., Smith, K. M., Veyrat, M., Mazzanti, M., Ramasseul, R., Marchon, J. C., Takeuchi, T., Goddard, W. A., III, and Shelnutt, J. A. (1995) *J. Am. Chem. Soc. 117*, 11085−11097.

32. Li, X. Y., Czernuszewicz, R. S., Kincaid, J. R., and Spiro, T. G. (1989) *J. Am. Chem. Soc. 111*, 7012−7023.

33. Alden, R. G., Crawford, B. A., Doolen, R., Ondrias, M. R., and Shelnutt, J. A. (1989) *J. Am. Chem. Soc. 111*, 2070−2072.

34. Howes, B. D., Schiodt, C. B., Welinder, K. G., Marzocchi, M. P., Ma, J.-G., Zhang, J., Shelnutt, J. A., and Smulevich, G. (1999) *Biophys. J. 77*, 478−492.

35. Hu, S., Morris, I. K., Singh, J. P., Smith, K. M., and Spiro, T. G. (1993) *J. Am. Chem. Soc. 115*, 12446−12458.

36. Lu, Y., Pauleta, S. R., Goodhew, C. F., Moura, I., Pettigrew, G. W., and Shelnutt, J. A. (2001) *Biochemistry* (submitted for publication).

37. Franco, R., Ma, J.-G., Lu, Y., Ferreira, G. C., and Shelnutt, J. A. (2000) *Biochemistry 39*, 2517−2529.

38. Jentzen, W., Ma, J. G., and Shelnutt, J. A. (1998) *Biophys. J. 74*, 753−763.

39. Ma, J.-G., Laberge, M., Song, X.-Z., Jentzen, W., Jia, S.-L., Zhang, J., Vanderkooi, J. M., and Shelnutt, J. A. (1998) *Biochemistry 37*, 5118−5128.

40. Jentzen, W., Song, X., and Shelnutt, J. A. (1996) *Biophys. J. 70*, A153.

41. Hu, S., Smith, K. M., and Spiro, T. G. (1996) *J. Am. Chem. Soc. 118*, 12638−12646.

42. Baumann, U., Wu, S., Flaherty, K. M., and McKay, D. B. (1993) *EMBO J. 12*, 3357−3364.

43. Kurumbail, R. G., Stevens, A. M., Gierse, J. K., McDonald, J. J., Stegeman, R. A., Pak, J. Y., Gildehaus, D., Miyashiro, J. M., Penning, T. D., Seibert, K., Isakson, P. C., and Stallings, W. C. (1996) *Nature 384*, 644−648.

44. Loll, P. J., Picot, D., Ekabo, O., and Garavito, R. M. (1996) *Biochemistry 35*, 7330−7340.

BI002870Z